International Journal of Engineering Research and Development
e- ISSN: 2278-067X, p-ISSN: 2278-800X, www.ijerd.com
Volume 22, Issue 5 (May 2026), PP 436-446

Performance evaluation of Nickel oxide catalyst in a Primary Reformer.

[1] Deinma, Sekibo [2] Akpa, J.G [3] Dagde, K.K.
[1, 2, 3,] *Department of Chemical/Petrochemical Engineering, Faculty of Engineering, Rivers State University, Nigeria*

Abstract
Nickel-based catalysts remain the industrial standard for steam methane reforming because of their high activity and economic viability; however, their long-term performance in primary reformers is severely constrained by progressive deactivation arising from sintering, carbon deposition, and impurity poisoning. These degradation processes reduce active surface area, alter reaction selectivity, and increase energy demand, yet industrial catalyst management is still largely based on empirical maintenance and replacement schedules rather than predictive, mechanistic degradation models. This limitation restricts the implementation of condition-based maintenance strategies and optimized turnaround planning. Consequently, there is a need for quantitative frameworks that link NiO catalyst effectiveness and degradation kinetics to reformer performance metrics such as methane conversion, hydrogen yield, and thermal utilization. This study aims to study the effectiveness and degradation behaviour of a nickel oxide catalyst in the primary reformer unit of the Haber–Bosch ammonia synthesis process. A comprehensive mathematical model was developed to describe reforming reaction kinetics and mass balances while incorporating catalyst effectiveness and deactivation phenomena. The primary reformer was represented as a one-dimensional packed-bed reactor operating under steady-state plug-flow conditions, consisting of furnace-heated tubes filled with spherical NiO-based catalyst pellets, consistent with industrial reformer configurations. Methane consumption on the catalyst surface was described using a simplified irreversible Langmuir–Hinshelwood kinetic expression showing the dependence of reaction rate on methane and steam partial pressures while accounting for surface adsorption effects. Intraparticle diffusion limitations were incorporated through the Thiele modulus, with the resulting reduction in observable reaction rate quantified using the effectiveness factor. Catalyst deactivation was modeled as the combined effect of coke deposition and thermal sintering, expressed as the multiplicative contribution of individual activity decay functions. Catalyst poisoning was assumed negligible for model simplicity. Coke-induced deactivation was represented by an exponential decay function relating coke accumulation to the progressive loss of accessible active sites, while sintering was modeled as a time-dependent exponential decay reflecting irreversible nickel particle growth at reforming temperatures. The coupled mass balance, energy balance, diffusion, and activity decay equations were solved using a sequential ODE-based numerical strategy implemented in MATLAB. Simulation results showed that methane concentration decreased from an initial value of 1.0 $\mathrm{mol}.L^{-1}$ in a near-exponential manner, confirming first-order kinetic behaviour with faster consumption at higher concentrations. The effectiveness factor declined continuously as the Thiele modulus increased from φ = 0.05 to 30, with $\eta \approx 1$ under kinetically controlled conditions ($\varphi \ll 1$) and approaching zero in diffusion-limited regimes ($\varphi \gg 1$). Catalyst activity commenced near unity ($\alpha \approx 1$) at t = 0 due to the pristine catalyst state and a fixed moderate initial coke loading (C_c = 0.4), exhibiting an initial plateau followed by a smooth decline governed by combined coking and sintering effects, with a curvature parameter n = 0.6. By approximately 2.8 h, activity had declined significantly but remained above zero, indicating sustained residual functionality. Coke formation rates were highest at early times (t ≈ 0–5 h), decreased markedly over t ≈ 5–30 h due to progressive site blocking captured by an $\exp(-\beta t)$ term, and approached an asymptotic low-rate regime over 30–55 has active site availability became limiting. The simulated temperature dependence of methane conversion showed rapid increases at lower temperatures and gradual curvature at higher temperatures, consistent with industrial observations for Ni-based reforming catalysts operating above 700 K. Parametric analysis revealed that methane conversion increased monotonically with steam–carbon ratio from 1.2 to 5.0, approaching an asymptotic maximum. At low steam–carbon ratios (S/C ≈ 1.2–1.8), conversion remained limited to approximately 0.45–0.60 due to insufficient steam availability and enhanced carbon formation via methane cracking and the Boudouard reaction, resulting in active site blockage. At intermediate ratios (S/C ≈ 2–3.2), methane conversion increased sharply to approximately 0.75–0.85 as higher steam partial pressures enhanced reforming kinetics, suppressed coke formation through gasification, and restored active surface coverage. At higher steam–carbon ratios (S/C ≥ 3.5), conversion approached an asymptotic range of 0.90–0.95, reflecting diminishing returns due to thermodynamic equilibrium and heat-transfer constraints, while residual sintering-related deactivation prevented complete conversion.

Keywords: *Nickel oxide catalyst, steam methane reforming, primary reformer, catalyst deactivation, coke deposition, sintering, hydrogen production, effectiveness factor, Thiele modulus, Langmuir–Hinshelwood kinetics, methane conversion, packed-bed reactor.*

Date of Submission: 13-05-2026 Date of acceptance: 28-05-2026

I. INTRODUCTION

Ammonia (NH_3) is a colourless, highly reactive gas with a characteristic pungent odour and significant toxicity in high concentrations. It plays a critical role in the global chemical industry as the primary precursor for nitrogen-based fertilisers and many other nitrogen-containing compounds (Er *et al.,* 2024). Naturally, ammonia is generated in the environment mainly through the anaerobic decomposition of biomass, such as plant and animal matter, and via biological nitrogen fixation in leguminous plants through symbiotic rhizobia bacteria (Janović & Jukić, 2018).

Commercially, the production of ammonia is overwhelmingly dominated by the industrially developed Haber–Bosch process, in which atmospheric nitrogen (N_2) is reacted with hydrogen (H_2) over an iron-based catalyst at elevated temperature (typically 400–500 °C) and high pressure (above 100 bar), with recycling of unreacted gases to improve efficiency. The underlying reaction;

$$N_2 + 3H_2 \rightarrow 2NH_3 \quad (1)$$

is exothermic and favoured at high pressures and relatively moderate temperatures, consistent with Le Châtelier's principle for equilibrium shifts (Britannica Editors, 2025).

Historically, the process was pioneered by Fritz Haber, who demonstrated ammonia synthesis in the lab around 1909, and then industrialised by Carl Bosch under the auspices of BASF, with the first large-scale plants commencing operations in the 1910s (Janović & Jukić, 2018). For these achievements Haber was awarded the Nobel Prize in Chemistry in 1918, and Bosch received the Prize in 1931 in recognition of their pioneering development of high-pressure chemical synthesis methods (Britannica Editors, 2025).

Despite over a century of incremental improvements, the core chemistry and reactor configuration developed during the early 20th century remain fundamentally unchanged today. According to the International Fertiliser Association, the original high-pressure iron-catalyst configuration is still the basis of all modern ammonia synthesis plants, although mechanical, heat-integration and catalyst surface technologies have been improved. Recent reviews note that while process intensification efforts (such as electro-ammonia synthesis and smaller modular units) are underway, the conventional Haber–Bosch loop continues to undergird the global ammonia industry (Er *et al.,* 2024).

The enduring importance of the Haber–Bosch process arises from its role in enabling large-scale fertiliser manufacture, which in turn has supported global food production and population growth throughout the 20th and 21st centuries (Er *et al.,* 2024). However, this reliance also underscores critical challenges: the process consumes large amounts of energy and hydrogen feedstocks (traditionally from fossil fuels), and remains one of the most significant industrial contributors to greenhouse-gas emissions (Er *et al.,* 2024). Thus, while the historical development of the Haber–Bosch process represents a landmark of industrial chemistry, ongoing research aims to enhance catalyst performance, reduce energy demand and enable lower-temperature or ambient-pressure ammonia synthesis routes

Ammonia Synthesis

Ammonia (NH_3) synthesis is one of the most significant industrial chemical processes, serving as the backbone for the global production of fertilizers, explosives, plastics, and pharmaceuticals. The primary industrial route for synthesizing ammonia is the Haber-Bosch process, which combines nitrogen (N_2) and hydrogen (H_2) gases under high temperature and pressure in the presence of a catalyst. This process accounts for over 150 million tonnes of ammonia production annually and consumes about 1–2% of global energy output (Appl, 2011).

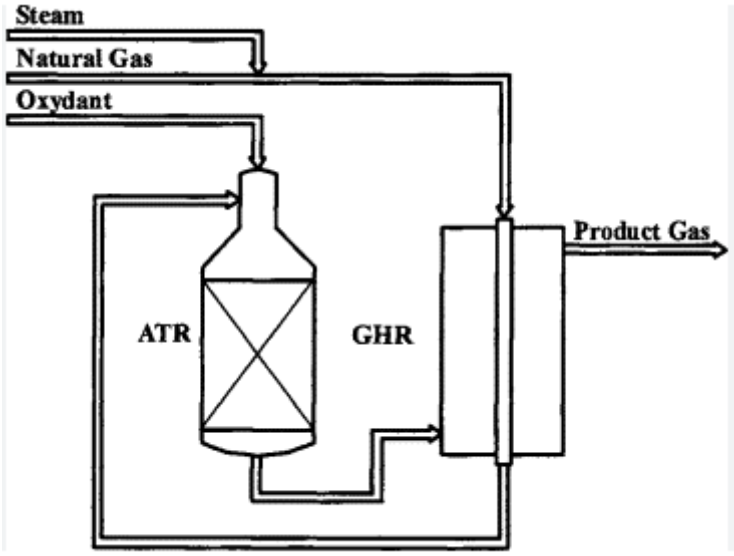

Figure 1: Schematics of a Steam Reformer

A critical stage in ammonia synthesis is the primary reforming process, where natural gas (primarily methane) is reformed with steam to produce synthesis gas (a mixture of hydrogen, carbon monoxide, and carbon dioxide). This process occurs over nickel-based catalysts, particularly Nickel Oxide (NiO) supported on alumina. The effectiveness of these catalysts directly influences the efficiency, selectivity, and energy consumption of the overall Haber-Bosch process (Rostrup-Nielsen & Christiansen, 2011).

The catalytic performance of NiO in reforming reactions is largely determined by factors such as catalyst dispersion, resistance to sintering, sulfur poisoning, and thermal stability. Over time, catalysts may become "spent" due to structural changes or contamination, resulting in decreased activity and selectivity (Forzatti & Lietti, 1999). Evaluating the effectiveness of spent versus fresh catalysts is crucial for optimizing reformer operation and reducing process costs.

Despite the widespread use of NiO catalysts, the continuous demand for energy-efficient and environmentally sustainable ammonia production necessitates further investigation into their long-term performance. This project proposal aims to assess the performance degradation and catalytic behavior of Nickel Oxide catalysts in the primary reformer, contributing to improved process modeling, catalyst design, and plant reliability.

II. EXTENT OF PAST WORKS

Nickel-based catalysts remain the industrial benchmark for steam methane reforming (SMR), the main hydrogen production step feeding the Haber–Bosch ammonia synthesis loop. Their performance determines methane conversion, hydrogen yield, energy efficiency, and catalyst lifetime in the primary reformer. Recent studies emphasize both catalytic activity and long-term stability under high-temperature operating conditions (Meloni, 2020; Rostrup-Nielsen & Sehested, 2017). Hydrogen generation is a critical upstream operation in the Haber–Bosch process, as the stoichiometric synthesis of ammonia requires a hydrogen-to-nitrogen ratio of approximately 3:1. Contemporary ammonia plants obtain most of their hydrogen from steam methane reforming (SMR), which re mains the dominant industrial route globally. According to the International Energy Agency (2021), more than 70% of worldwide hydrogen production is derived from natural gas reforming, underscoring the central role of the primary reformer in enabling large-scale ammonia synthesis.

In a typical Haber–Bosch plant configuration, the primary reformer performs the first stage of methane conversion by reacting desulfurized natural gas with high-pressure steam over a nickel-based catalyst. The main reactions are highly endothermic, requiring substantial heat input from external burners to sustain temperatures in the range of 750–900 °C (Rostrup-Nielsen & Christiansen, 2011). These temperatures shift the equilibrium of the steam reforming reaction ($CH_4 + H_2O \rightleftharpoons CO + 3H_2$) toward hydrogen formation, making the reformer a major energy consumer within the ammonia production chain. The thermal intensity and harsh operating conditions dictate not only the choice of catalyst but also the design of furnace geometry, reformer tubes, and heat-transfer configurations. Commercial practice consistently favours nickel-oxide-derived catalysts—most commonly NiO dispersed on γ-Al_2O_3—because nickel offers an optimal balance between catalytic activity, cost, and mechanical robustness (Jones et al., 2019; Meloni, 2020). Compared with noble metals such as rhodium or ruthenium, nickel is more economically viable for large-scale deployment. Furthermore, the NiO/Al_2O_3 system provides a

combination of strong metal–support interactions, thermal stability, and resistance to mechanical degradation during the severe thermal cycles typical of reformer startups and shutdowns. During initial operation, NiO is reduced in situ to metallic Ni, which then acts as the active catalytic phase responsible for C–H bond activation in methane molecules (Bartholomew, 2001).

Thermodynamic influences on carbon formation define the broad operating envelope in which coking is either suppressed or becomes inevitable. At the most basic level, the propensity for solid carbon to form from gaseous reactants is governed by the relative free energies of the gas- and solid-phase species: lower steam-to-carbon (S/C) ratios shift the reaction environment toward more reducing conditions and reduce the chemical potential of oxidizing species (H_2O, OH*), thereby making methane cracking and related carbon-forming equilibria thermodynamically more favorable (Wang *et al.,* 2018; Meloni, 2020). Likewise, high partial pressures of hydrocarbons (e.g., elevated CH_4 concentration or the presence of heavier hydrocarbons/tars in biomass/biogas feeds) increase the activity of carbon-forming reactions and move the system closer to the carbon-stable side of the phase diagram (Singh, 2024; Szablowski, 2025). These trends explain why industrial practice uses S/C ratios well above stoichiometric values (commonly 2.5–3.5 for SMR) when processing variable or impurity-bearing feeds—to provide a thermodynamic buffer against coke onset (Wang *et al.,* 2018; Ganguli, 2023). Among the various poisons encountered in industrial practice, sulfur-containing species are the most detrimental due to their strong chemical affinity for metallic nickel. Even at trace concentrations, typically at the parts-per-million (ppm) or sub-ppm level, sulfur compounds can significantly suppress reforming activity by permanently blocking active metal sites and altering the electronic structure of the catalyst surface (Subramani*et al.,* 2019). As a result, sulfur poisoning imposes strict requirements on feedstock purity and pretreatment in hydrogen and syngas production systems.

Sulfur enters the reformer feed primarily in the form of hydrogen sulfide (H_2S) or organic sulfur compounds such as mercaptans, thiophenes, and sulfides that originate from natural gas, refinery off-gases, or biogas streams. Upon contact with metallic Ni^0, these species dissociatively adsorb and react to form stable nickel sulfide phases (Ni_xS_γ). The formation of nickel sulfide is thermodynamically favored under reforming conditions and effectively removes surface nickel atoms from participation in methane activation and reforming reactions. Because the Ni–S bond is significantly stronger than the Ni–C or Ni–H bonds, sulfur adsorption is exceptionally persistent, and even very low sulfur coverages can cause disproportionate losses in catalytic activity (Boscherini *et al.,* 2023).

From a mechanistic perspective, sulfur poisoning reduces catalyst performance through several coupled effects. First, sulfur atoms occupy and block Ni ensembles required for C–H bond cleavage in methane, thus lowering intrinsic reaction rates. Second, sulfur modifies the electronic properties of neighboring Ni atoms, decreasing their ability to adsorb and activate reactant molecules even when not directly covered. Third, sulfur adsorption can promote secondary deactivation pathways, including enhanced carbon deposition and accelerated sintering, by disrupting normal surface chemistry and metal–support interactions (Huang, *et al.,* 2010). These effects collectively explain why SMR catalysts exhibit dramatic activity losses at sulfur concentrations that would be considered negligible for many other catalytic processes.

The impact of sulfur poisoning is often partially irreversible under standard reforming conditions. While limited regeneration may be achieved at high temperatures in strongly reducing or oxidizing environments, complete removal of sulfur from Ni surfaces is rarely feasible without compromising catalyst structure through sintering or oxidation. Consequently, industrial reforming operations prioritize sulfur prevention rather than remediation. This has led to the widespread implementation of stringent upstream feed purification systems, including hydrodesulfurization (HDS), zinc oxide (ZnO) guard beds, and adsorptive polishing units designed to reduce sulfur levels to well below 0.1 ppm before entering the primary reformer (Huang *et al.,* 2010).

III. MATERIALS AND METHOD

2.1 Materials Used

The following materials will be used in this research project:

i. Plant Operational data
ii. MATLAB Software
iii. Literature data

2.2 Method Used

2.3 Mathematical Modeling of the Primary Reformer

The primary reformer is modeled as a one-dimensional packed-bed reactor operated under steady plug-flow conditions. The catalyst bed consists of spherical NiO-based catalyst pellets packed in tubes and externally heated by a furnace.

Consider a differential axial slice of the packed bed of length dz and cross-sectional area A as shown in figure 2:

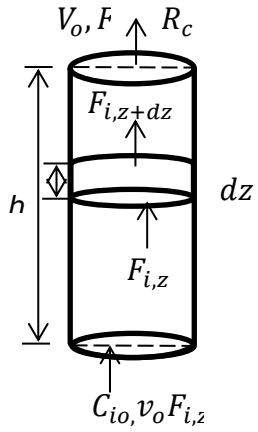

Figure 2: Schematics of a Packed Bed Reformer

Where;
$F_i(z)$ = molar flow of species i into position z
$F_i(z + dz)$ = molar flow of species i out of position z
Within a differential cross sectional area of the packed-bed primary reformer, catalytic reactions take place on nickel-based catalyst pellets, where reactant molecules are first transported from the bulk gas phase to the external surface of the pellets and subsequently diffuse into the pellet pores to reach active nickel sites. As operation proceeds, the intrinsic activity of the catalyst progressively declines due to concurrent deactivation mechanisms, notably carbon deposition (coking), thermal sintering of nickel particles, and poisoning by trace impurities in the feed. Simultaneously, the strongly endothermic steam-methane reforming reactions require continuous heat input, which is supplied by external firing across the reactor tubes. This infinitesimal reactor segment therefore constitutes the fundamental control volume upon which the coupled mass, energy, and catalyst activity balances that govern primary reformer performance are formulated.

2.3.1 Mass Balance of Species in the Primary Reformer

For species i, the general conservation statement over a differential control volume is:

$$\begin{bmatrix}\text{Rate of inflow of}\\ \text{species A into the}\\ \text{differential volume}\end{bmatrix} = \begin{bmatrix}\text{Rate of outflow of species}\\ \text{A out of differential volume}\end{bmatrix} + \begin{bmatrix}\text{Rate of depletion of species}\\ \text{A due to chemical reaction}\\ \text{in differential volume}\end{bmatrix} + \begin{bmatrix}\text{Rate of Accumulation}\\ \text{of species A in differential volume}\end{bmatrix} \quad (2)$$

Under steady state condition, the accumulation term of equation (3.1) becomes zero, therefore, equation (3.1) reduces to:

$$0 = \begin{bmatrix}\text{Rate of inflow of}\\ \text{species A into the}\\ \text{differential volume}\end{bmatrix} - \begin{bmatrix}\text{Rate of outflow of species}\\ \text{A out of differential volume}\end{bmatrix} + \begin{bmatrix}\text{Rate of depletion of species}\\ \text{A due to chemical reaction}\\ \text{in differential volume}\end{bmatrix} \quad (3)$$

Equation (3) can be written as:

$$0 = F_i(z) - F_i(z + dz) + R_i A dz \quad (4)$$

Where;
$F_i(z) =$ rate of inflow of species i into the cross section
$F_i(z + dz) =$ rate of outflow of species i from the cross section
$R_i =$ rate of formation or consumption of species i per reactor volume [mol·m^{-3}·s^{-1}]
$A =$ cross sectional area
$dz =$ distance
Dividing through equation (3.3) by dz and taking limit as $dz \rightarrow 0$yields;

$$\frac{dF_i}{dz} = AR_i \quad (5)$$

In the primary reformer only the solid catalyst fraction contributes to reaction. Therefore, the volumetric reaction rate is defined as:

$$R_i = (1 - \varepsilon_b) r_i \quad (6)$$

where;
$\varepsilon_b =$ bed porosity (-)
$r_i =$ reaction rate per catalyst volume

The observed reaction rate is reduced relative to intrinsic kinetics due to intraparticle diffusion limitation and catalyst deactivation, thus the reaction rate per catalyst volume (r_i) is written as:

$r_i = \alpha(z,t)\eta r_i^{int}$ (7)

Where;

$\alpha(z,t) =$ catalyst activity (0 – 1)

$\eta =$ effectiveness factor which accounts for intraparticle diffusion

$r_i^{int} =$ intrinsic kinetic rate

Substituting equation (7) into (6) and then into equation (5) yields;

$\frac{dF_i}{dz} = A(1-\varepsilon_b)\alpha(z,t)\eta r_i^{int}$ (8)

Equation (3.7) is the governing mass balance equation for each reacting species in the primary reformer.

2.3.2 Intrinsic Reaction Rate

Steam methane reforming over nickel-based catalysts is commonly described using Langmuir–Hinshelwood–type kinetics, which account for surface adsorption of reactants and the competitive occupation of active sites by gaseous species. In this study, a simplified irreversible Langmuir–Hinshelwood rate expression is adopted to represent the intrinsic consumption rate of methane on the catalyst surface. This formulation captures the essential dependence of the reaction rate on the partial pressures of methane and steam while incorporating adsorption effects through a denominator that reflects surface coverage by reacting and non-reacting species. The resulting intrinsic kinetic expression for steam methane reforming is therefore given as:

$CH_4 + H_2O \leftrightarrow CO + 3H_2$ (9)

$CO + H_2O \leftrightarrow CO_2 + H_2$ (10)

$r_{CH_4}^{int} = k_{SMR}\frac{P_{CH_4}P_{H_2O}}{\left(1+\sum_j K_j P_j\right)^2}$ (11)

with Arrhenius temperature dependence;

$k_{SMR} = A_{SMR}exp\left(-\frac{E_{SMR}}{RT}\right)$ (12)

This formulation accounts for adsorption effects while maintaining one-directional simplicity (Xu & Froment, 1989; Fogler, 2016).

2.3.3 Intraparticle Diffusion (Effectiveness)

Thiele modulus

To account for the influence of intraparticle diffusion on the apparent reaction rate within porous catalyst pellets, the Thiele modulus is introduced as a dimensionless parameter comparing the relative rates of chemical reaction and molecular diffusion. For a spherical catalyst pellet, the Thiele modulus is defined:

$\emptyset = R_p\sqrt{\frac{k_{app}}{D_{eff}}}$ (13)

Where;

k_{app} = apparent rate constant

D_{eff} = diffusivity

R_p = particle

Effectiveness factor for Spherical Pellets

The extent to which internal diffusion limitations reduce the observable reaction rate is subsequently accounted for through the effectiveness factor, which relates the actual overall reaction rate to the rate that would be achieved in the absence of diffusion resistance. For spherical catalyst pellets undergoing first-order or pseudo–first-order kinetics, the effectiveness factor is expressed as:

$\eta = \frac{3}{\emptyset^2}\left(\frac{\emptyset}{\tanh\emptyset} - 1\right)$ (13)

This approach incorporates intraparticle diffusion without solving full radial PDEs and is standard for packed-bed reactors (Fogler, 2016).

2.4 Catalyst Deactivation Modeling

2.4.1 Overall activity

To represent the combined influence of multiple deactivation pathways on catalyst performance, the overall catalyst activity is defined as the product of individual activity functions associated with coking, sintering, and poisoning, giving as:

$\alpha = \alpha_{coke}.\alpha_{sint}.\alpha_{pois}$ (14)

In the course of this work, it is assumed that since the purity of the reacting species is relatively high, the decline in catalyst activity due to catalyst poisoning is negligible when compared to that of coke deposition and sintering. Thus, equation (3.14) becomes;

$$\alpha = \alpha_{coke}.\alpha_{sint} \quad (15)$$

2.4.2 Coke induced Deactivation

Carbon deposition on nickel active sites is modeled using an empirical kinetic expression that relates the rate of coke formation to temperature and local reactant availability, particularly methane and steam, as expressed in Equation (3.16).

$$\frac{dC_c}{dt} = k_c exp\left(-\frac{E_c}{RT}\right)\frac{P_{CH_4}}{(1+K_{CH_4}P_{H_2O})} \quad (16)$$

Activity decay due to coke:

The resulting loss in catalytic activity due to coke accumulation is described by an exponential decay function that links the coke loading on the catalyst to the reduction in available active sites, as shown in Equation (17).

$$\alpha_{coke} = \exp(-\beta_c C_c) \quad (17)$$

2.4.3 Sintering-induced deactivation

Thermal sintering of nickel particles, which leads to irreversible loss of active surface area at reforming temperatures, is represented by a time-dependent exponential decay in catalyst activity, as given by Equation (3.18).

$$\alpha_{sint} = \exp(-k_s t)^n \quad (18)$$

The rate of catalyst deactivation by coke deposition on the catalyst active sites and sintering due to continuous exposure to high temperature can be obtained by combining equation (16) - (18) which is written as:

$$\frac{dC_c}{dt} = k_c exp\left(-\frac{E_c}{RT}\right)\frac{P_{CH_4}}{(1+K_{CH_4}P_{H_2O})}\alpha_{coke}.\alpha_{sint} \quad (19)$$

2.4.4 Objective Function

The overall equation describing steam reforming of methane over Nickel – based catalyst in a primary reformer can be described by substituting necessary parameters into equation (3.7);

$$\frac{dF_i}{dz} = A(1-\varepsilon_b)\alpha(z,t)\eta r_i^{int} \quad (20)$$

2.5 Energy Balance for a Primary Reformer

For the differential element Adz:

$$Accumulation = Input - Output + Heat\ added + Heat\ of\ Reaction \quad (21)$$

Under steady state condition, the accumulation term in equation (3.18) becomes zero, hence:

$$0 = \dot{m}C_pT(z) - \dot{m}C_pT(z+dz) + Q_{ht}Adz - \sum_r(\Delta H_r R_r Adz) \quad (22)$$

Dividing equation (3.22) by Adz and simplifying yields:

$$\rho_g u C_p \frac{dT}{dz} = Q_{ht}(1-\varepsilon_b)\alpha\eta\sum_r(r_r^{int}\Delta H_r) \quad (23)$$

This equation shows that temperature changes along the reformer are governed by the competition between external heat input and endothermic reaction demand (Rostrup-Nielsen & Sehested, 2017).

IV. RESULTS AND DISCUSSION

3.1: Concentration Profiles of Constituents in a Primary Reformer

The concentration profile of methane (CH_4) exhibits adecrease over the simulation timeframe of 0 to 50 minutes as shown in Figure 3. At time zero, the methane concentration begins at its initial value of 1.0 mol/L and progressively declines as the reaction proceeds. This decrease reflects the gradual consumption of methane by the reforming reaction and is characteristic of first-order reaction kinetics, where the reaction rate is directly proportional to the concentration of the reactant (Fogler, 2016). The near-exponential nature of the decline indicates that methane is consumed more rapidly at early times when its concentration is high and slows as the available methane diminishes.

Reports on reactor kinetics often characterizes this behavior as expected for elementary first-order reactions under isothermal, well-mixed conditions (Levenspiel, 1999). Studies by García-Trinidad *et al.,* (2020) examining methane conversion in packed bed reactors report similar decreasing CH_4 profiles at the onset of reforming.

The CO concentration profile rises from zero at $t = 0$ to a finite plateau as time increases. This trend is consistent with the stoichiometric generation of one mole of CO for every mole of CH_4consumed. The increase is initially steep, indicating rapid formation corresponding to the high rate of methane consumption early in the process. As the CH_4feedstock becomes depleted, the formation rate of CO decreases, resulting in a leveling off of

the CO concentration. This plateauing effect suggests that the system approaches a quasi-steady state where the net accumulation of CO slows as the reactant reservoir diminishes (Smith & Missen, 2021).

Comparative studies on methane reforming report CO concentration trends that follow similar rising behavior before approaching a pseudo-steady state as reactions equilibrate (Shahid *et al.,* 2020).

The profile for hydrogen(H_2)also demonstrates a monotonic increase from zero, but at a noticeably higher rate than CO owing to its stoichiometric coefficient of three in the reaction. For each mole of CH_4 consumed, three moles of $H_2$are produced; therefore, the H_2 concentration increases approximately three times faster relative to CO in the initial phases of the reaction. The hydrogen concentration continues to rise throughout the simulation, albeit at a decreasing rate as available CH_4decreases. This behavior reflects the higher yield of H_2per mole of $CH_4$and aligns with industrial expectations where steam reforming serves as a major source of hydrogen production (Rostrup-Nielsen & Sehested, 2002).

Experimental investigations, such as those by Ermanoski *et al.,* (2022), similarly observe rapid increases in H_2concentration during early reforming stages, followed by a gradual stabilization as reaction kinetics slow due to reactant depletion.

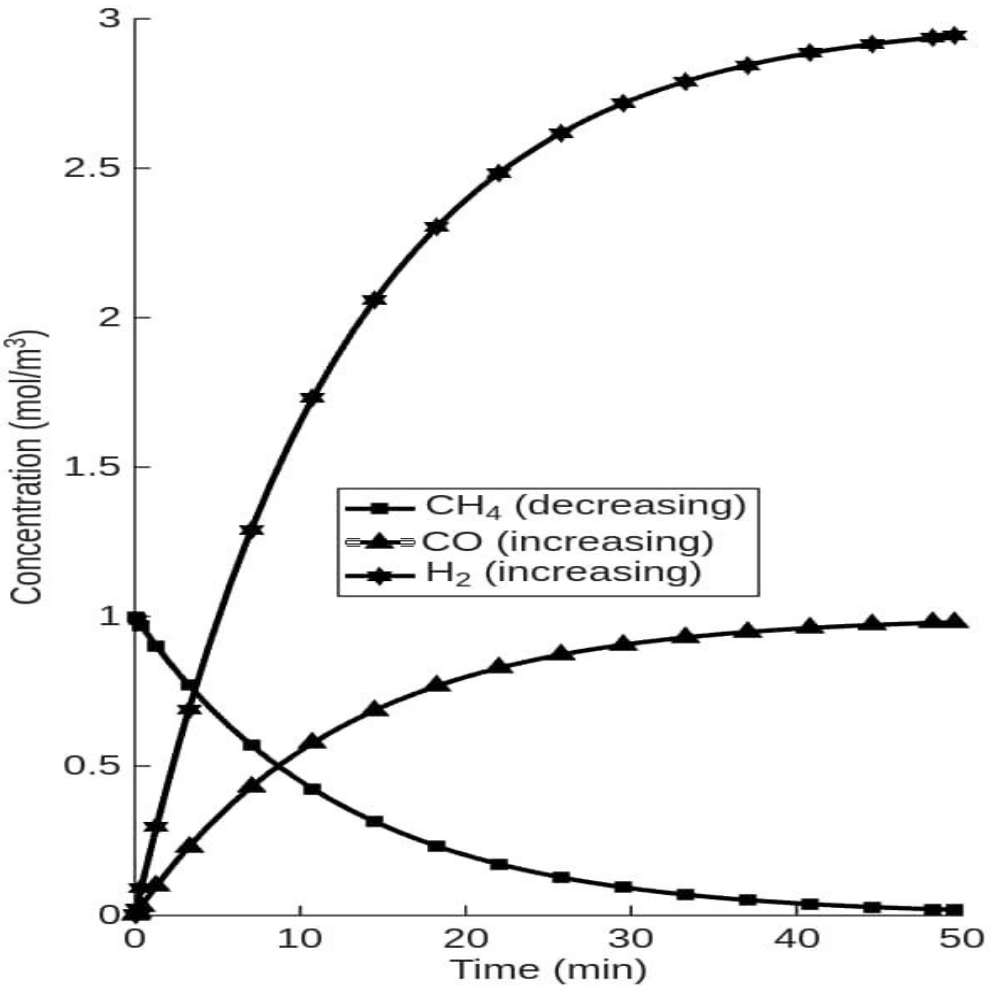

Figure 3: Concentration profiles of CH_4, CO and H_2

3.2: Effect of Effectiveness Factor in the Reformer

In heterogeneous catalytic systems, the effectiveness factor *(η)* is a fundamental parameter that quantifies how efficiently a porous catalyst particle utilizes its internal surface area under reaction conditions. The effectiveness factor represents the ratio between the actual, pore-averaged rate of reaction and the rate that would be achieved if the entire catalyst volume reacted at the surface reactant concentration. Its value is strongly influenced by the balance between intrinsic kinetics *and* internal diffusion resistance within catalyst pores.

As shown in Figure 4.2, the effectiveness factor η declines continuously as the Thiele modulus φ increases from 0.05 to 30. At very low φ values ($\varphi \ll 1$), η approaches a value close to unity; conversely, at high

φ values (φ ≫ 1), η tends toward values near zero. This monotonic decline indicates a transition from a regime where reaction rate controls the overall performance to a regime dominated by internal diffusion resistance.

At φ values less than about 1, the effectiveness factor remains near 1, indicating that the reactants readily diffuse through the catalyst pores, and the catalyst operates under intrinsic kinetic control. In this region, reactants are able to penetrate uniformly into the catalyst particle, and the reaction at internal sites is not limited by diffusion. These features reflect the conditions where the rate of diffusion sufficiently exceeds the rate of reaction, allowing the reactant concentration inside the particle to remain close to that at the surface.

As φ increases beyond unity, η begins to decrease more rapidly. This decline signifies the increasing significance of diffusion resistance: the reaction rate becomes faster relative to the rate at which reactants diffuse into the interior of the catalyst, leading to depletion of reactants near the pore interior and lower average reaction rates. For large φ, the effectiveness factor asymptotically approaches small values, indicating that only a superficial layer of the catalyst near the external surface contributes significantly to the overall reaction.

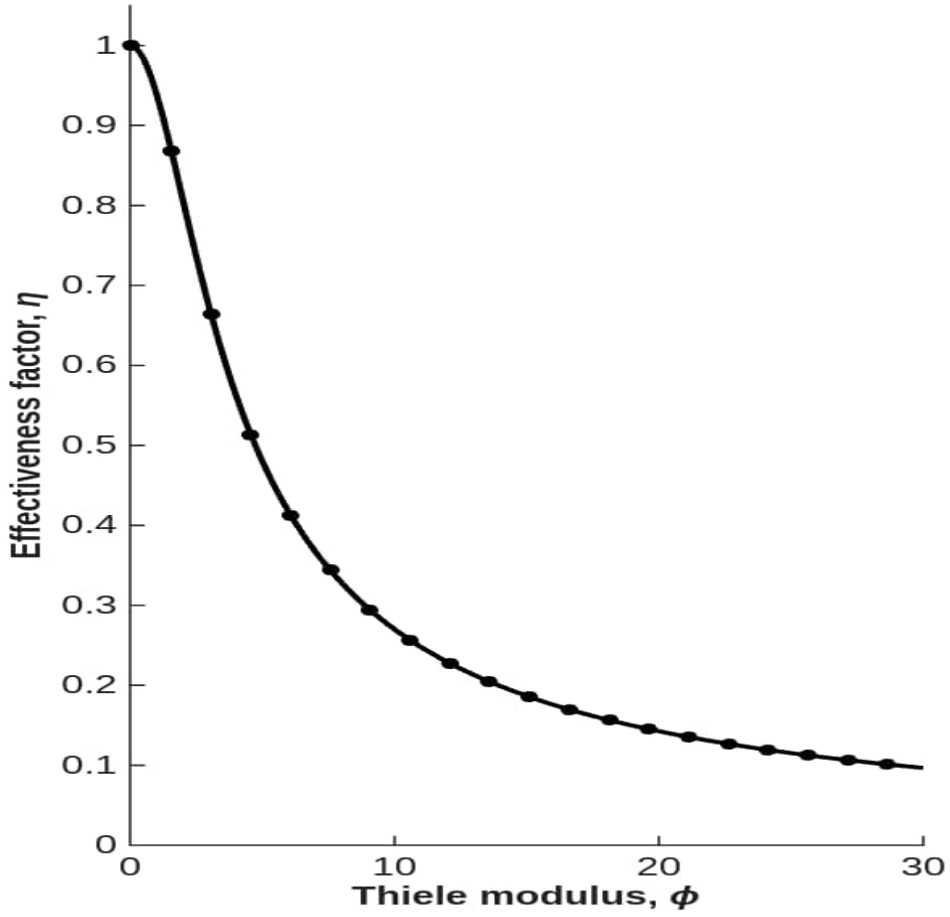

Figure 4: Effect of Effectiveness Factor in the Reformer

IV. CONCLUSION

In this study, the primary reformer was represented as a one-dimensional packed-bed reactor operating under steady-state plug-flow conditions. The reactor comprises furnace-heated tubes filled with spherical NiO-based catalyst pellets, reflecting the physical configuration of industrial steam methane reformers. Methane consumption on the catalyst surface was described using a simplified irreversible Langmuir–Hinshelwood kinetic expression, which adequately captures the dependence of the reaction rate on the partial pressures of methane and steam while accounting for surface adsorption phenomena through a coverage-dependent denominator. The influence of internal mass transfer resistance within the porous catalyst pellets was incorporated through the introduction of the Thiele modulus, serving as a dimensionless measure of the relative rates of intrinsic chemical reaction and intraparticle diffusion. The resulting reduction in the observable reaction rate due to diffusion limitations was quantified using the effectiveness factor, which relates the actual overall reaction rate to the hypothetical rate in the absence of internal diffusion resistance.

To account for the combined impact of catalyst deactivation mechanisms on reformer performance, the overall catalyst activity was formulated as the multiplicative contribution of individual activity functions associated with coking, sintering, and poisoning. For model simplicity, the contributions from catalyst poisoning was assumed to be negligible and therefore excluded from further analysis. Catalyst deactivation due to coke formation was modeled using an exponential decay function that relates coke accumulation to the progressive loss of accessible active sites. Thermal sintering of nickel particles, an irreversible phenomenon at reforming temperatures was represented by a time-dependent exponential decay in catalyst activity reflecting the gradual loss of active surface area. The final deactivation model was obtained by coupling the effects of coke deposition and sintering, yielding a model describing catalyst activity decay in the primary reformer.

A sequential ODE-based numerical solution strategy was successfully implemented in MATLAB to solve the coupled mass-balance, activity-decay, intraparticle-diffusion, and energy-balance equations developed in Sections 3.2–3.5, yielding physically consistent trends that support the validity of the proposed model. The methane concentration decreased from its initial value of $1.0\ mol\ L^{-1}$ in a near-exponential manner, confirming first-order kinetic behaviour in which consumption is fastest at high initial concentrations and progressively slows as methane is depleted. Intraparticle diffusion effects were reflected by a continuous decline in the effectiveness factor as the Thiele modulus increased from $\varphi = 0.05$ to 30, with $\eta \approx 1$ at very low φ ($\varphi \ll 1$) and approaching zero at high φ ($\varphi \gg 1$), indicating a transition from kinetic to diffusion-limited regimes. Catalyst activity commenced near unity ($\alpha \approx 1$) at t = 0 due to the pristine state of the catalyst and a fixed moderate initial coke loading ($C_c = 0.4$), with an initial plateau suggesting negligible early deactivation; as time progressed, α decreased smoothly under the combined influence of coke coverage and sintering, governed by a curvature parameter n = 0.6, capturing the gradual and cumulative nature of experimentally observed deactivation. By approximately 2.8 h, activity had declined significantly but remained above zero, indicating persistent residual functionality consistent with practical reforming operations. Coke formation kinetics exhibited a high initial rate($t \approx 0 - 5$ h), characteristic of abundant available active sites and kinetic control, followed by a marked decline during $t \approx 5 - 30$ h due to progressive site blocking incorporated through the exponential decay term $exp(-\beta t)$, and finally an asymptotic low-rate regime over 30–55 h where further deposition became limited primarily by active-site availability rather than intrinsic kinetics. In addition, the simulated temperature dependence of methane conversion showed a rapid increase in the lower temperature range and a gradual curvature at higher temperatures, qualitatively consistent with industrial observations for Ni-based primary reforming catalysts operating above 700 K, where enhanced surface reaction rates and adsorption–desorption dynamics dominate and equilibrium limitations progressively emerge.

The study provides the following contributions to knowledge:

i. This work developed and implemented a comprehensive primary reformer model that simultaneously couples methane reforming kinetics, intraparticle diffusion (via the Thiele modulus and effectiveness factor), catalyst deactivation (coking and sintering), and energy balance. This integrated approach advances existing models, which often treat these phenomena separately, and provides a more realistic predictive tool for primary reformer performance.

ii. This study quantitatively demonstrated how catalyst activity (α), coke formation rate, and effectiveness factor (η) evolve with time and operating conditions, explicitly showing the transition from kinetically controlled to diffusion- and deactivation-influenced regimes.

REFERENCES

[1]. Bartholomew, C. H. (2001). Mechanisms of catalyst deactivation. *Applied Catalysis A: General*, *212*(1-2), 17-60.

[2]. Boscherini, M., Storione, A., Minelli, M., Miccio, F., & Doghieri, F. (2023). New perspectives on catalytic hydrogen production by the reforming, partial oxidation and decomposition of methane and biogas. *Energies*, *16*(17), 6375.

[3]. Citaristi, I. (2022). International energy agency—iea. In *The Europa directory of international organizations 2022* (pp. 701-702). Routledge.

[4]. Enayatizade, H., Chahartaghi, M., Hashemian, S. M., Arjomand, A., & Ahmadi, M. H. (2019). Techno-economic evaluation of a new CCHP system with a hydrogen production unit. *International Journal of Low-Carbon Technologies*, *14*(2), 170-186.

[5]. Esfandiary, M., Karimi, N., & Saedodin, S. (2024). Maximization of hydrogen production via methane steam reforming in a wavy microreactor by optimization of catalyst coating: A combined computational and data analytics approach. *Industrial & Engineering Chemistry Research*, *63*(43), 18599-18614.

[6]. Fogler, H. S. (1999). *Elements of chemical reaction engineering*. Pearson Educacion.

[7]. Ganguli, A., & Bhatt, V. (2023). Hydrogen production using advanced reactors by steam. *Role of Mathematical Modeling in Advanced Power Generation Systems*.

[8]. Hou, K., & Hughes, R. (2001). The kinetics of methane steam reforming over a Ni/α-Al2O catalyst. *Chemical Engineering Journal*, *82*(1-3), 311-328.

[9]. Huang, C., Huang, X., & Rodgers, M. (2010). Impurity mitigation strategies. *Proton Exchange Membrane Fuel Cells: Contamination and Mitigation Strategy (H. Li, S. Knights, Z. Shi, JW Van Zee, and J. Zhang, eds.). CRC Press Taylor & Francis Group*, 339-400.

[10]. Khan, M. A. (2021). *Utilizing modeling tools to design a reactor and a catalyst for dry reforming of methane* (Doctoral dissertation).

[11]. Li, S., & Gong, J. (2014). Strategies for improving the performance and stability of Ni-based catalysts for reforming reactions. *Chemical Society Reviews*, *43*(21), 7245-7256.

[12]. Li, X., Chen, L., & Wang, Y. (2023). Modeling of steam reforming reactors with catalyst deactivation for hydrogen production. *International Journal of Hydrogen Energy*, 48(5), 2187–2199.

[13]. Meloni, E., Martino, M., & Palma, V. (2020). A short review on Ni based catalysts and related engineering issues for methane steam reforming. *Catalysts*, *10*(3), 352.
[14]. Nguyen, T., Luu, C. L., Phan, H. P., Nguyen, P. A., & Van Nguyen, T. T. (2020). Methane dry reforming over nickel-based catalysts: insight into the support effect and reaction kinetics. *Reaction Kinetics, Mechanisms and Catalysis*, *131*(2), 707-735.
[15]. Pafili, A., Charisiou, N. D., Douvartzides, S. L., Siakavelas, G. I., Wang, W., Liu, G., ... & Goula, M. A. (2021). Recent progress in the steam reforming of bio-oil for hydrogen production: a review of operating parameters, catalytic systems and technological innovations. *Catalysts*, *11*(12), 1526.
[16]. Rahman, M. A., Ahmed, S. S., & Hossain, M. M. (2022). Modeling and performance assessment of nickel-based catalysts for methane steam reforming. *Chemical Engineering Journal*, 428, 131–148.
[17]. Richter, J., Rachow, F., Israel, J., Roth, N., Charlafti, E., Günther, V., ... & Mauss, F. (2023). Reaction mechanism development for methane steam reforming on a Ni/Al2O3 catalyst. *Catalysts*, *13*(5), 884.
[18]. Rouwenhorst, K. H., Travis, A. S., & Lefferts, L. (2022). 1921–2021: A Century of renewable ammonia synthesis. *Sustainable Chemistry*, *3*(2), 149-171.
[19]. Salcedo, A., Lustemberg, P. G., Rui, N., Palomino, R. M., Liu, Z., Nemsak, S., ... & Irigoyen, B. (2021). Reaction pathway for coke-free methane steam reforming on a Ni/CeO2 catalyst: active sites and the role of metal–support interactions. *ACS catalysis*, *11*(13), 8327-8337.
[20]. Shen, Z., Nabavi, S. A., & Clough, P. T. (2024). Intrinsic kinetics of steam methane reforming over a monolithic nickel catalyst in a fixed bed reactor system. *Chemical Engineering Science*, *299*, 120482.
[21]. Silva, J., Rocha, C., Soria, M. A., & Madeira, L. M. (2022). Catalytic steam reforming of biomass-derived oxygenates for H2 production: a review on Ni-based catalysts. *Chem Engineering*, *6*(3), 39.
[22]. Song, C., & Pan, W. (2024). Advances in catalytic materials for hydrogen and ammonia synthesis. *Frontiers in Catalysis*, 5, 117–129.
[23]. Subramani, V., Sharma, P., Zhang, L., & Liu, K. (2009). Catalytic steam reforming technology for the production of hydrogen and syngas. *Hydrogen and syngas production and purification technologies*, 14-126.